



# A NOVEL TRANSFORMERLESS SINGLE-STAGE BRIDGELESS CONVERTER CHARGER ENHANCING POWER QUALITY FOR LIGHT ELECTRIC VEHICLES

<sup>1</sup> Tadiparthi Nirmala Nidhi, <sup>2</sup> Md.Khajafarid, <sup>3</sup> Balu Badhavathu, <sup>4</sup> Meda Spandana, <sup>5</sup> Erra Ramesh

<sup>1,2,3</sup> Assistant Professor, <sup>4,5</sup> Students

Department of EEE

Vaagdevi College of Engineering, Warangal, Telangana

## ABSTRACT:

This paper presents an innovative design for a transformerless single-stage bridgeless converter-based charger aimed at improving power quality for light electric vehicles (LEVs). With the growing demand for efficient charging solutions in the electric vehicle market, traditional charging methods often lead to power quality issues, including harmonics and voltage fluctuations. The proposed charger utilizes a single-stage conversion process, significantly reducing the number of components and associated losses while maintaining high efficiency. By employing a bridgeless configuration, the design minimizes conduction losses and enhances overall performance. Simulation and experimental results demonstrate that the proposed charger effectively mitigates power quality issues, providing a stable and clean power supply for LEVs. Additionally, the charger complies with international standards for power quality, making it a viable solution for modern electric vehicle charging infrastructure. This research contributes to the ongoing development of advanced charging technologies, promoting the adoption of light electric vehicles and supporting the transition to sustainable transportation systems.

DOI Number: [10.48047/nq.2022.20.8.nq221179](https://doi.org/10.48047/nq.2022.20.8.nq221179)

NeuroQuantology 2022;20(8):11397-11406

## I. INTRODUCTION

The rapid growth of the electric vehicle (EV) market has led to an increasing demand for efficient and reliable charging solutions, particularly for light electric vehicles (LEVs) such as electric scooters, bicycles, and small cars. Traditional charging systems often rely on transformer-based designs, which, while effective, can introduce several challenges related to power quality, including harmonics, voltage fluctuations, and increased energy losses. These issues not only affect the performance of the charging stations but can

also impact the longevity and efficiency of the vehicles being charged.

To address these challenges, there is a growing interest in transformerless charger designs that provide a more compact, efficient, and cost-effective solution. A promising approach is the development of single-stage bridgeless converters, which eliminate the need for bulky transformers while maintaining the benefits of high efficiency and reduced component count. The bridgeless configuration further minimizes conduction losses by allowing current to flow through fewer components, which is





particularly advantageous for applications in light electric vehicles that require lightweight and compact charging solutions.

This paper aims to present a novel transformerless single-stage bridgeless converter-based charger that significantly improves power quality for LEVs. The proposed design not only optimizes the charging process but also enhances the overall performance of the system by addressing common power quality issues associated with traditional charging methods. Through detailed analysis, simulation, and experimental validation, this study explores the advantages of the proposed charger configuration, demonstrating its effectiveness in delivering stable and clean power for light electric vehicle applications.

The findings of this research contribute to the ongoing development of advanced charging technologies, facilitating the widespread adoption of electric vehicles and supporting the transition towards more sustainable transportation systems. By focusing on improving power quality, this work highlights the potential for innovative solutions to enhance the user experience and operational efficiency of light electric vehicles, paving the way for a greener future.

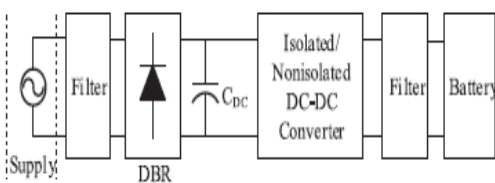


Fig. 1. Structure of conventional charger configurations for LEVs.

the charger [2]. The single-phase active power factor correction (APFC) methods are extensively utilized to eliminate the abovementioned drawbacks of the

conventional low power rating chargers. In an APFC method, a dc–dc converter is employed between DBR and CDC, to improve the supply-side performances of the charger from a power quality point of view. It is noteworthy that an APFC converter can perform multiple tasks in a charger based on the configuration of a charger, i.e., single-stage chargers or double-stage chargers. In a double-stage configuration, an APFC is employed to fulfill supply-side requirements and another dc–dc converter is required for satisfying the load-side demands, whereas only an APFC dc–dc converter performs both the tasks in the single-stage chargers. Several two-stage charger configurations based on different APFC solutions have been explored for the EVs/LEVs charging applications [3]–[5]. However, each solution has its benefits and drawbacks regarding its device count [6], conduction and switching losses [7], control complexities [5], and efficiency [8]. In order to improve the charger’s efficiency by reducing its conduction losses in the APFC stage, many bridgeless APFC converters with partial [9] or complete [10] elimination of the DBR have been reported in the literature. A detailed review of bridgeless APFC converters is given in [11]. Recently, some bridgeless integrated charging solutions have been suggested to improve the component count and losses in the chargers while retaining the advantages of the two-stage chargers [12], [13]. In an integrated configuration, the semiconductor devices have been shared by both dc–dc converters, which reduce the device count and associate losses. However, the increased control complexities and high device stresses make them less attractive for LEVs applications. The ripple-free charging current is considered as a major advantage of a single-phase two-stage charger. However, several authors have claimed that low-frequency ripples in the charging current, if controlled





properly, do not affect performance of the battery [14], [15].

While addressing these drawbacks of two-stage chargers, several researchers have provided various single-stage charger configurations for the EVs/LEVs along with enhanced power quality at the supply side [16], [17]. The single-stage chargers have high power density [18], less component count [19], and a simplified control structure [20]. Moreover, a properly designed single-stage charger configuration can provide better efficiency than its two-stage counterpart. The limited output voltage capability of the conventional boost converter and the high distortion in the supply current near the zero crossing in the conventional buck converter [21] rule out the possibilities of their application as an APFC in the single-stage LEVs chargers. Therefore, in most of the cases, the shortcomings of buck and boost derived converters are eliminated by employing the buck–boost derived converters such as buck–boost, Cuk, SEPIC, Zeta, CSC, and Luo dc–dc converters. The Cuk dc–dc converter shows excellent input and output current ripple characteristics among all buck–boost dc–dc converters [22]. However, the conventional buck–boost dc–dc converters are less suitable to provide a transformerless single-stage charging solution for the LEVs, due to their limited gain capability. In the case of LEVs, due to low battery voltage, the transformerless charger configuration operates at a very low duty ratio, which ultimately affects the charger's dynamic performance and efficiency [23]. Therefore, most of the single-stage LEVs chargers based on conventional dc–dc converters require a transformer for getting the desired dc voltage gain. However, the inclusion of the transformer increases the cost and size of the charger. Moreover, the leakage inductance of the transformer increases the voltage stress across the devices [24]. Consequently, the

development of the single-stage transformerless charger for the EVs is gaining the researcher's attention nowadays [25]. However, the improved power quality based transformerless charger configuration for the LEVs is still rarely addressed by the researchers. Several efforts have been made recently to improve the voltage gain capability of conventional dc–dc converters such as by utilizing coupled inductors, by cascading of converters, by employing quadratic converters, by considering multiplier circuit, interleaved front end structure, and switched inductor or hybrid switched inductor–capacitor structure [26]. In the case of coupled inductors, operating characteristics of the converter largely depend upon the coupling coefficient whereas the cascading and multiplier approach in converters increases the component count, which leads to higher cost, low efficiency, and complex circuitry. However, the quadratic converter provides higher efficiency than cascaded converter at the cost of increased voltage and current stresses [27]. In order to overcome these issues, a switching dual network based on split capacitors or split inductors along with two to three diodes is proposed in [28]. The switched inductor (SI) and switched capacitor (SC) networks efficiently modify the dc gain of conventional converters, based on the series/parallel charging and parallel/series discharging of the capacitors or inductors. In [29], an SI Cuk PFC converter based charger is proposed for LEVs. However, this charger has a high cost, complex control, and has increased size of magnetic components due to CCM



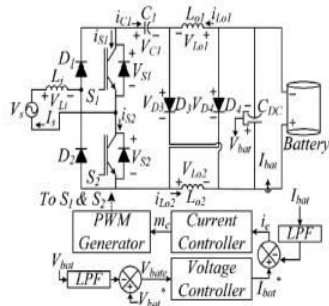


Fig. 2. BSIC PFC converter based transformerless charger configuration.

operation. Moreover, the DBR at the front side increases the conduction losses and component count in the charger. An enhanced power quality charger based on a single-stage configuration of BSIC PFC converter is presented in this work.

Main contributions of this article are highlighted as follows.

- 1) This charger provides a single-stage charging solution for the LEVs, without having a transformer or coupled inductors with minimum component counts.
- 2) The design and control of the BSIC converter are carried out under the DCM condition, which not only reduces the size of magnetic components and associated losses but it also reduces the sensor requirements. Furthermore, the DCM operation rules out the need for the PLL system, and therefore, it considerably simplifies the control implementation part.
- 3) The bridgeless structure at the front side reduces total device counts and the conduction losses of the charger.
- 4) Additionally, the enhanced power quality operation of the charger is tested and verified over a wide range of supply voltage while implementing the constant-current and constant-voltage charging modes.
- 5) A comparative analysis of the presented charger configuration with a conventional Cuk PFC converter [4] and an SI Cuk PFC converter [29] is carried out and presented based on

various factors, e.g., number of components, control complexities, cost, size, and supply-side performances.

## II. BATTERY CHARGER CONFIGURATION

The single-phase single-stage charger configuration based on the BSIC PFC converter is depicted in Fig. 2.

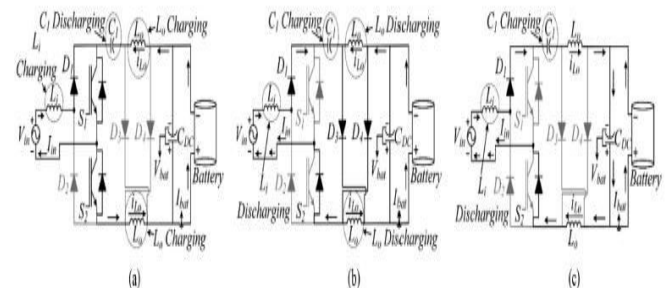


Fig. 3. Operating modes of bridgeless switched inductor Cuk PFC converter in a switching cycle (positive half-cycle). (a) Mode-P(I) ( $t_1-t_2$ ), (b) Mode-P(II) ( $t_2-t_3$ ), (c) Mode-P(III) ( $t_3-t_4$ ).

This configuration implements a single-phase single-stage transformerless ac-dc converter for the LEVs charging application with additional high step-down gain capabilities and improved power quality performances at the supply side. The bridgeless structure at the front side is supplied by a single-phase supply with a nominal voltage ( $V_s$ ) rating of 220 V, 50 Hz. The input inductor ( $L_1$ ) serves the purpose of the Cuk converter input inductor as well as it acts as a filter for the supply current ( $I_s$ ). The forward leg of the front-end bridge constitutes of two diodes  $D_1$  and  $D_2$ , while the second leg consists of two active switches  $S_1$  and  $S_2$ , unlike the conventional DBR, which has the combination of four diodes.  $D_1$  and  $D_2$  operate for the positive and negative half-cycles of supply voltage, respectively, whereas both switches ( $S_1$  and  $S_2$ ) are switched simultaneously irrespective of supply voltage polarity to reduce the control complexities. The intermediate capacitor ( $C_1$ ) serves a similar purpose as the conventional Cuk PFC converter. At the load side, an SI network is provided, which consists of a combination of two inductors ( $L_{o1}$  and  $L_{o2}$ )





and two diodes (D3 and D4). The overall gain of the charger is improved by series charging and parallel discharging of the output inductors. A battery having a capacity of 100 Ah with a nominal voltage of 48 V is considered as a load. Furthermore, minimum sensing devices are utilized while implementing the control of the charger, which in turn reduces the control complexities and cost of the charger.

#### OPERATING PRINCIPLE OF CHARGER

This section describes the working principle of the charger. The symmetrical structure of the charger results in symmetrical operation during each half-cycle of supply. It is assumed that the converter operates in a steady-state condition with lossless active and passive components. Moreover, the value of  $V_s$  is considered as invariable ( $V_{in}$ ), during a switching cycle, due to high switching to the line frequency ratio. Despite having low-frequency ripples, it is assumed that battery current ( $I_{bat}$ ) and voltage ( $V_{bat}$ ) are constant in a switching cycle. Moreover,  $L_{o1}$  and  $L_{o2}$  are assumed to have equal inductance ( $L_o$ ), so

$$\begin{aligned} L_{o1} &= L_{o2} = L_o \\ V_{L_{o1}} &= V_{L_{o2}} = V_{L_o} \\ I_{L_{o1}} &= I_{L_{o2}} = I_{L_o} \end{aligned} \quad (1)$$

The three operating modes during the positive half-cycle are discussed as Mode P(I)–P(III) and shown in Fig. 3.

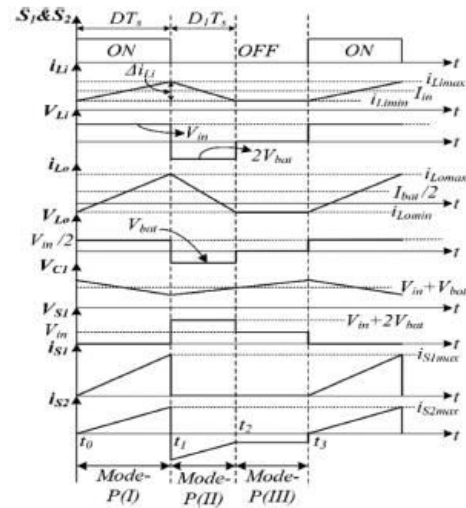


Fig. 4. Waveform of different states over a switching cycle.

#### A. Mode-P(I) ( $t_0$ - $t_1$ )

Prior to starting of this mode, the input ( $i_{Li}$ ) and output ( $i_{Lo}$ ) inductor currents have equal and opposite magnitudes, as shown in Fig. 4. Moreover, D3 and D4 are in reverse biased condition. This mode starts by turning ON switches S1 and S2 simultaneously, as shown in Fig. 3(a). The output inductors ( $L_{o1}$  and  $L_{o2}$ ) start charging by the stored energy of the intermediate capacitor C1, i.e., C1 is in discharging mode whereas  $L_i$  is charged by the supply voltage. The supporting equations for this mode are as follows:

$$V_{L_i} = L_i \cdot (di_{L_i}/dt) = V_{in} \quad (2)$$

$$L_i = (V_{in} \cdot D \cdot T_s) / \Delta i_{L_i} \quad (3)$$

$$V_{L_{o1}} = L_{o1}(di_{L_{o1}}/dt), V_{L_{o2}} = L_{o2}(di_{L_{o2}}/dt) \quad (4)$$

$$V_{L_{o1}} = V_{L_{o2}} = (V_{C1} - V_{bat})/2 \quad (5)$$

$$I_{C1} = C_1 \cdot (dv_{C1}/dt) = -I_{L_o} \quad (6)$$

This mode ends when S1 and S2 are turned OFF





### B. Mode-P(II) (t1-t2)

As the switch is turned OFF, D3 and D4 are clamped to a positive voltage and start conducting, as shown in Fig. 3(b). C1 starts charging by the input current ( $i_{Li}$ ) and the inductor currents, i.e.,  $i_{Li}$  and  $i_{Lo}$  start decaying to zero with a negative slope, as depicted in Fig. 4. The associated mathematical expressions are shown as follows:

$$V_{Li} = V_{in} - V_{C1} - V_{bat} \quad (7)$$

$$V_{Lo1} = V_{Lo2} = -V_{bat}/2 \quad (8)$$

$$I_{C1} = I_{Li}. \quad (9)$$

This mode ends at an instant ( $t_2$ ) when  $i_{Li}$  is equal and opposite of the current in output inductors, i.e.,  $i_{Lo}$ . Finally, D3 and D4 stop conducting and converter enters into freewheeling mode.

### C. Mode-P(III) (t2-t3)

In most cases, this mode is referred to as the freewheeling mode. The duration of this mode depends on the loading condition, switching frequency, and the value of output inductors of the converter. During this mode, both switches and diodes stop conducting, as shown in Fig. 3(c). The voltage across the  $L_i$  and  $L_o$  is zero, as shown in Fig. 4:

$$V_{Li} = 0, V_{Lo} = 0 \quad (10)$$

$$I_{C1} = C_1 \cdot (dv_{C1}/dt) = I_{Li} \quad (11)$$

$$I_{Co} = C_o \cdot (dv_{bat}/dt) = -(I_{Li} + I_{bat}). \quad (12)$$

It is noteworthy that only D1 conducts for a half-cycle unlike conduction of two diodes in conventional DBR-based chargers. From (1)–(12), the dc voltage gain ( $M$ ) and the average voltage across the C1 ( $V_{C1}$ ) are calculated by the volt-sec balance principle and is given by

$$V_{bat} = V_{in} \cdot D/(2 \cdot D_1) = M \cdot V_{in} \quad (13)$$

$$V_{C1} = V_{bat} \cdot (1 + (2D_1/D)) = V_{in} + V_{bat} \quad (14)$$

where D1 represents the diodes (D5 and D6) duty ratio, as shown in Fig. 4, and  $M$  is the gain of the converter, i.e.,  $V_{bat}/V_{in}$ . In a switching cycle, average current in output inductors, i.e.,  $I_{Lo}$ , is half of the average battery current ( $I_{bat}$ ), and is written as

$$I_{Lo} = I_{bat}/2 = (1/T_s) \int_0^{T_s} i_{Lo}(t) \cdot dt \quad (15)$$

$$I_{Lo} = I_{bat}/2 = [V_{bat} \cdot D_1 \cdot (D + D_1)]/(2f_s \cdot L_o) \quad (16)$$

$$I_{bat} = V_{bat}/R_L \quad (17)$$

where  $f_s$  is the converter's switching frequency and  $R_L$  is the fictitious load resistance. From (16) and (17), D1 is obtained as

$$D_1 = \{(L_o \cdot f_s)/[R_L \cdot (1 + 2 \cdot M)]\}^{(1/2)}. \quad (18)$$

The condition for the DCM operation is given as  $D + D_1 < 1$  (19)

$$D_1 \cdot (1 + 2 \cdot M) < 1 \quad (20)$$

$$D_1 < 1/(1 + 2 \cdot M). \quad (21)$$

For the critical conduction case

$$D_{1critical} = 1/(1 + 2 \cdot M). \quad (22)$$

From (18) and (22), the output inductors minimum value, i.e.,  $L_{ocritical}$  is calculated as

$$D_{1critical}^2 = \{(L_{ocritical} \cdot f_s)/[R_L \cdot (1 + 2 \cdot M)]\} \quad (23)$$

$$\frac{1}{(1 + 2 \cdot M_{max})^2} = \frac{L_{ocritical} \cdot f_s}{R_{Lmin} \cdot (1 + 2 \cdot M_{max})} \quad (24)$$

$$L_{ocritical} = R_{Lmin}/[f_s \cdot (1 + 2 \cdot M_{max})]. \quad (25)$$

The value of  $L_o$  at the boundary of CCM and DCM operations is provided in (25). So, while selecting the output inductors, it is to be ensured that the selected value must be lower than the calculated value to implement the DCM operation of the charger over the defined range.

### III. DESIGN OF CHARGER CONFIGURATION

This charger configuration is designed to operate for a broad range of  $V_s$ , i.e., from 130 V ( $V_{smin}$ ) to 260 V ( $V_{smax}$ ). The DCM mode of operation reduces the size of the output





inductors. A power rating (Pmax) of 850 W is considered for the design of the charger. The variation of battery voltage (Vbat) from low SOC to full SOC is considered from 45 V (Vbatmin) to 65 V (Vbatmax), for maximizing the safety and reliability of the charger, throughout the different modes of the charging. The BSIC converter dc voltage gain is given by (13) as

$$V_{bat} = V_{in} \cdot D / (2 * D_1) = M \cdot V_{in}. \quad (26)$$

Therefore, for a complete line cycle, Vin can be written as

$$V_{in} = \sqrt{2} \cdot V_s \cdot |\sin(\omega t)|. \quad (27)$$

By considering, input and output voltage limits, the dc voltage gain (M) varies from 0.1224 (Mmin) to 0.354 (Mmax). Moreover, by taking maximum efficiency into account, the fictitious load resistance (RL) varies from 2.38 Ω (RLmin) to 4.97 Ω (RLmax).

#### A. Selection of Lo1 Lo2 in DCM

The selection of output inductors is made using (25) as

$$L_{ocritical} = R_{Lmin} / [f_s \cdot (1 + 2 \cdot M_{max})]. \quad (28)$$

The switching frequency (fs) is considered as 20 kHz. Therefore, the critical value of Lo1 and Lo2 is given as

$$L_{ocritical} = 2.38 / [20k \cdot (1 + 2 \cdot 0.354)] = 69.7 \mu H.$$

Since the selected value should be less than the calculated value, Lo1 and Lo2 having an inductance of 40 μH are selected during the implementation of the converter.

#### B. Selection of Li in CCM

The design of Li is carried out in CCM mode and the required value, which ensures CCM operation throughout the operation of the charger, is calculated as

$$V_{Li} = L_i \cdot (di_{Li}/dt) = V_{in} \quad (29)$$

$$L_i = (V_{in} \cdot D) / (\chi \cdot I_{Li} \cdot f_s) = (V_{in}^2 \cdot D) / (\chi \cdot I_{Li} \cdot f_s) \quad (30)$$

where Rin is the fictitious input resistance of the charger, χ is the allowable percentage current ripples, and D is the duty ratio. From (18) and (26), the range of duty ratios (D), i.e., Dmin and Dmax, is calculated as follows:

$$D_{max} = 2 \cdot M_{max} \cdot \sqrt{(L_o \cdot f_s) / (R_{Lmax} \cdot (1 + 2 \cdot M_{max}))} \quad (31)$$

$$D_{min} = 2 \cdot M_{min} \cdot \sqrt{(L_o \cdot f_s) / (R_{Lmin} \cdot (1 + 2 \cdot M_{min}))}. \quad (32)$$

From (31) and (32), Dmax and Dmin are obtained as 0.2174 and 0.1271, respectively. By considering 30% current ripple, i.e., χ = 0.30, the critical value of Li, i.e., Licritical, is given as

$$L_{icritical} = \frac{V_{inmax}^2 \cdot D_{max}}{P_{max} \cdot \chi \cdot f_s} = \frac{(\sqrt{2} \cdot V_{smax})^2 \cdot D_{max}}{P_{max} \cdot \chi \cdot f_s} \quad (33)$$

$$L_{icritical} = \frac{(\sqrt{2} \cdot 260)^2 \cdot 0.2174}{850 \cdot 0.3 \cdot 20 \cdot 10^3} = 5.76 \text{ mH}.$$

Therefore, to ensure CCM operation, Li is selected as 6 mH.

#### C. Selection of C1 in CCM

The selection of C1 is critical because of two different restrictions on the capacitor voltage profile. In a switching cycle, the voltage across C1 should be constant, whereas, in a complete line cycle, the voltage should follow the supply voltage profile. Therefore, the value of C1 is calculated as

$$C_1 = 1 / \{ \omega_{res}^2 \cdot (L_i + L_{o1} + L_{o2}) \}. \quad (34)$$

where wres defines the frequency of resonance between C1, Li, Lo1, and Lo2. The selected wres should be high enough to the line frequency but lower than the switching frequency:

$$C_1 = 1 / \{ (2 \cdot \pi \cdot 2000)^2 \cdot (6m + 2 \cdot 40\mu) \} = 1.1 \mu F.$$

The selected value of C1 is 0.94 μF.

#### D. Selection of CDC

CDC is designed to minimize the flow of low-frequency ripple power into the battery, during charging without exceeding defined voltage ripple limit (λ) [22]. The size of CDC is mainly decided by the power and voltage handling limit





set as per application requirement. CDC is calculated as

$$C_{DC} = P_{max} / (4\pi \cdot f_{Line} \cdot \lambda \cdot V_{batmax}^2) \quad (35)$$

where fline is the supply frequency. Considering 3% ripple, CDC is calculated as

$$C_{DC} = 850 / (4\pi \cdot 50 \cdot 0.03 \cdot (65)^2) = 10.66 \text{ mF.}$$

Therefore,  $C_{DC}$  is taken as 11.75 mF.

#### IV. CONTROL TECHNIQUE

The BSIC converter is controlled to achieve two main objectives by incorporating minimum cost and complexities during the implementation. The prime objective of the controller is to control the charging current to the battery in CC and CV modes, as per the requirement. In addition to that, low distortion in supply current along with unity power factor operation at the supply side is another important objective of the control. The overall control is implemented by a conventional dual loop structure, as given in Fig. 2, using Texas Instruments (TI) TMS320F28377S DSP. The outer loop is employed to tackle the variations in Vbat whereas the inner loop takes care of Ibat while maintaining the UPF operation with minimum supply current distortions. For the outer loop, Vbat is sensed by utilizing a voltage sensor, and the switching frequency ripples are filtered out from it by employing a low-pass filter (LPF). In order to get the reference battery current (Ibat\*), the filtered Vbat is matched with Vbat, i.e., Vbat\*, and the error (Vbate) is fed to a voltage proportional-integral (PI) controller. The output of voltage PI controller provides the required Ibat\*. The expressions for outer loop are given as

$$V_{bate}(k) = V_{bat}^*(k) - V_{bat}(k) \quad (36)$$

$$I_{bat}^*(k) = I_{bat}^*(k-1) + k_{pV} \{V_{bate}(k) - V_{bate}(k-1)\} + k_{iV} \cdot V_{bate}(k) \quad (37)$$

where  $k_{pV}$  is the proportional gain,  $k_{iV}$  is the integral gain of the voltage PI controller, and  $k$  is the  $k$ th sampling instant. For implementing inner loop control, the charging current Ibat is sensed through a current sensor and filtered by an LPF. The filtered current is then compared with Ibat\* and the error (Ie) is passed through the current PI controller. The output of the PI controller provides the required duty ratio (mc) as

$$I_e(k) = I_{bat}^*(k) - I_{bat}(k) \quad (38)$$

$$m_c^*(k) = m_c^*(k-1) + k_{pI} \{I_e(k) - I_e(k-1)\} + k_{iI} \cdot I_e(k) \quad (39)$$

where  $k_{pI}$  and  $k_{iI}$  are, respectively, the proportional and integral constants of the current PI controller. The duty ratio (mc) is then compared with a sawtooth carrier waveform. The comparison provides the required gate drive signals for switches (S1 and S2). It is noteworthy that the switching signal is applied to S1 and S2, simultaneously, to reduce the complexity of the control.

#### Pulse width Modulation

Pulse Width Modulation (PWM) is the most effective means to achieve constant voltage battery charging by switching the solar system controller's power devices. When in PWM regulation, the current from the solar array tapers according to the battery's condition and recharging needs consider a waveform such as this: it is a voltage switching between 0v and 12v. It is fairly obvious that, since the voltage is at 12v for exactly as long as it is at 0v, then a 'suitable device' connected to its output will see the average voltage and think it is being fed 6v - exactly half of 12v. So by varying the width of the positive pulse - we can vary the 'average' voltage.



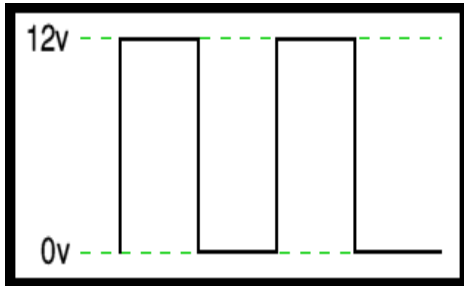


Fig.4.1 Average voltage exactly half of

12v

Similarly, if the switches keep the voltage at 12 for 3 times as long as at 0v, the average will be 3/4 of 12v - or 9v, as shown below.

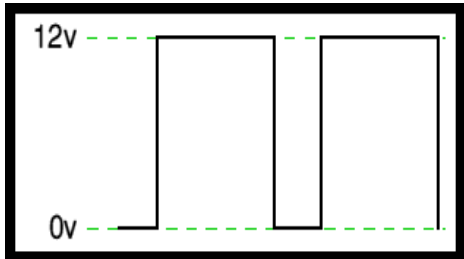


Fig.4.2 Average voltage will be 3/4 of

12v

and if the output pulse of 12v lasts only 25% of the overall time, then the average is

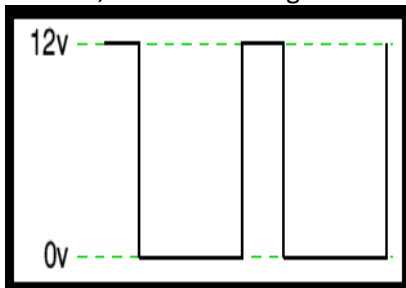


Fig.4.3 Average output voltage at 12v

By varying - or 'modulating' - the time that the output is at 12v (i.e. the width of the positive pulse) we can alter the average voltage. So we are doing 'pulse width modulation'. I said earlier that the output had to feed 'a suitable device'. A radio would not work from this: the radio would see 12v then 0v, and would probably not work properly. However a device such as a motor will respond to the average, so PWM is a natural for motor control.

## PI CONTROLLER

A variation of Proportional Integral Derivative (PID) control is to use only the proportional and integral terms as PI control. The PI controller is the most popular variation, even more than full PID controllers. The value of the controller output  $u(t)$  is fed into the system as the manipulated variable input.

$$e(t) = SP - PV$$

$$u(t) = u_{bias} + K_c e(t) + K_c I \int_0^t e(t) dt$$

The  $u_{bias}$  term is a constant that is typically set to the value of  $u(t)$  when the controller is first switched from manual to automatic mode. This gives "bumpless" transfer if the error is zero when the controller is turned on. The two tuning values for a PI controller are the controller gain,  $K_c$  and the integral time constant  $\tau_I$ . The value of  $K_c$  is a multiplier on the proportional error and integral term and a higher value makes the controller more aggressive at responding to errors away from the set point. The set point ( $SP$ ) is the target value and process variable ( $PV$ ) is the measured value that may deviate from the desired value. The error from the set point is the difference between the  $SP$  and  $PV$  and is defined as  $e(t) = SP - PV$

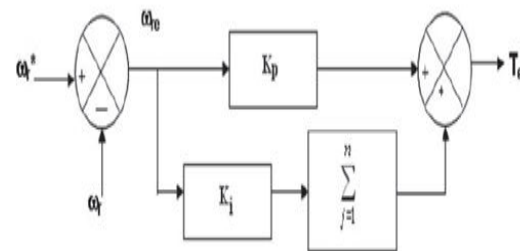


Fig.5.1. Block diagram of PI speed controller

V. Results:



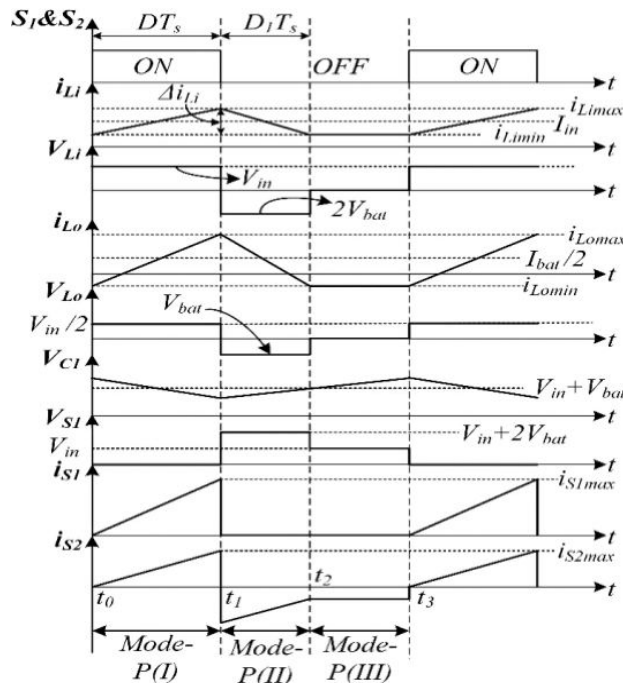


Fig: Simulation Waveforms

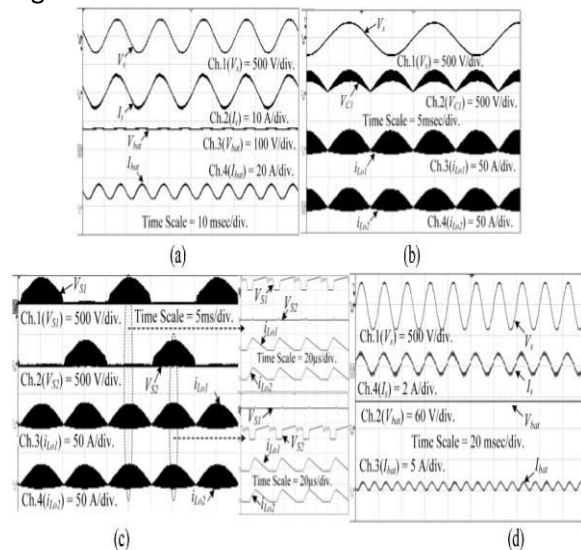


Fig: Generated Output Waveforms

## VI. CONCLUSION:

In conclusion, this research presents a transformative approach to charging light electric vehicles (LEVs) through the development of a transformerless single-stage bridgeless converter-based charger. By addressing the common power quality issues

associated with traditional charging systems, the proposed design effectively enhances efficiency, reduces component count, and minimizes conduction losses. The results from simulations and experimental validations demonstrate that the charger not only complies with international power quality standards but also provides stable and clean power supply essential for optimal LEV performance. This innovative charger configuration paves the way for more compact and cost-effective charging solutions, contributing to the broader adoption of electric vehicles and facilitating the transition toward sustainable transportation. Future work may focus on integrating advanced control strategies and energy management systems to further optimize the charging process, ensuring adaptability and resilience in diverse operational environments. Overall, this study underscores the potential of transformerless single-stage bridgeless converters in revolutionizing charging technology for light electric vehicles, fostering a cleaner and more efficient future for urban mobility.

## REFERENCES:

- [1] NITI Aayog and WEC, "Zero-emission vehicles: Towards a policy framework," NITI Aayog, New Delhi, India, Rep., 2008. [Online]. Available: [https://niti.gov.in/writereaddata/files/document\\_publication/EV\\_report.pdf](https://niti.gov.in/writereaddata/files/document_publication/EV_report.pdf)
- [2] Z. Yang and P. C. Sen, "Recent developments in high power factor switch-mode converters," in Proc. IEEE Can. Conf. Electron. Comp. Eng., Waterloo, ON, Canada, 1998, vol. 2, pp. 477–480.
- [3] H. Wang, S. Dusmez, and A. Khaligh, "A novel approach to design EV battery chargers using SEPIC PFC stage and optimal operating point tracking technique for LLC converter," in Proc. IEEE App. Power Electron. Conf. Expo., Fort Worth, TX, USA, 2014, pp. 1683–1689.





[4] R. Pandey and B. Singh, "A power-factor-corrected LLC resonant converter for electric vehicle charger using Cuk converter," *IEEE Trans. Indus. Appl.*, vol. 55, no. 6, pp. 6278–6286, Nov–Dec. 2019.

[5] D. Kim and B. Lee, "Asymmetric control algorithm for increasing efficiency of nonisolated on-board battery chargers with a single controller," *IEEE Trans. Veh. Technol.*, vol. 66, no. 8, pp. 6693–6706, Aug. 2017.

[6] A. V. J. S. Praneeth and S. S. Williamson, "A wide input and output voltage range battery charger using buck-boost power factor correction converter," in *Proc. IEEE Appl. Power Electron. Conf. Expo.*, Anaheim, CA, USA, 2019, pp. 2974–2979.

[7] S. Ryu, D. Kim, M. Kim, J. Kim, and B. Lee, "Adjustable frequency–duty cycle hybrid control strategy for full-bridge series resonant converters in electric vehicle chargers," *IEEE Trans. Indus. Electron.*, vol. 61, no. 10, pp. 5354–5362, Oct. 2014.

